

Article

Design of a Novel Compact Bandpass Filter Based on Low-Cost Through-Silicon-Via Technology

Hai Dong¹, Yingtao Ding¹, Han Wang¹, Xingling Pan¹, Mingrui Zhou¹ and Ziyue Zhang^{1,2,*} 

¹ School of Integrated Circuits and Electronics, Beijing Institute of Technology, Beijing 100081, China; 3420225025@bit.edu.cn (H.D.); ytd@bit.edu.cn (Y.D.); 3220215100@bit.edu.cn (H.W.); panxingling0705@163.com (X.P.); linghuaibu@163.com (M.Z.)

² BIT Chongqing Institute of Microelectronics and Microsystems, Chongqing 400030, China

* Correspondence: zyzzhang@bit.edu.cn

Abstract: Three-dimensional (3D) integration based on through-silicon-via (TSV) technology provides a solution to the miniaturization of electronic systems. In this paper, novel integrated passive devices (IPDs) including capacitor, inductor, and bandpass filter are designed by employing TSV structures. For lower manufacturing costs, polyimide (PI) liners are used in the TSVs. The influences of structural parameters of TSVs on the electrical performance of the TSV-based capacitor and inductor are individually evaluated. Moreover, with the topologies of capacitor and inductor elements, a compact third-order Butterworth bandpass filter with a central frequency of 2.4 GHz is developed, and the footprint is only 0.814 mm × 0.444 mm. The simulated 3-dB bandwidth of the filter is 410 MHz, and the fraction bandwidth (FBW) is 17%. Besides, the in-band insertion loss is less than 2.63 dB, and the return loss in the passband is better than 11.4 dB, showing good RF performance. Furthermore, as the filter is fully formed by identical TSVs, it not only features a simple architecture and low cost, but also provides a promising idea for facilitating the system integration and layout camouflaging of radio frequency (RF) devices.

Keywords: compact bandpass filter; integrated passive device (IPD); miniaturization; three-dimensional (3D) integration; through-silicon-via (TSV)



Citation: Dong, H.; Ding, Y.; Wang, H.; Pan, X.; Zhou, M.; Zhang, Z. Design of a Novel Compact Bandpass Filter Based on Low-Cost Through-Silicon-Via Technology. *Micromachines* **2023**, *14*, 1251. <https://doi.org/10.3390/mi14061251>

Academic Editor: Niall Tait

Received: 18 May 2023

Revised: 10 June 2023

Accepted: 13 June 2023

Published: 14 June 2023



Copyright: © 2023 by the authors. Licensee MDPI, Basel, Switzerland. This article is an open access article distributed under the terms and conditions of the Creative Commons Attribution (CC BY) license (<https://creativecommons.org/licenses/by/4.0/>).

1. Introduction

As one of the key components in radio frequency (RF) front ends and microwave systems, bandpass filters (BPFs) are extensively investigated and have spurred great advances in terms of structures, processes, and performance over the past decades. Several technologies such as low temperature co-fired ceramic (LTCC) [1,2], microstrip [3–6], substrate integrated waveguide (SIW) [7–9], and micro-electromechanical systems (MEMS) [10,11], are utilized to develop BPFs with specific characteristics such as broad bandwidth, high selectivity, low insertion loss, and compact size. Recently, with the rapid development of wireless communication, Internet of Things (IoT), and Artificial Intelligence (AI), the demands for miniaturization and integration of RF components are especially urgent, therefore, it is necessary to design filters that are more compact and easier to be integrated [12–15].

To achieve a smaller footprint, multi-layer structure and discriminating coupling are involved in the design of compact LTCC BPFs [16–18]. For SIW filters, some modified topologies such as the half-mode SIW (HMSIW) [19], and the ridge half-mode SIW (RHM-SIW) [20,21], are proposed to optimize the device size. Besides, based on the spoof surface plasmon polaritons (SSPPs) in the microwave frequencies, several novel compact wide-band SSPP filters [22,23] and hybrid SIW-SSPP filters [24,25] are developed for plasmonic systems, microwave circuits, and wearable devices. MEMS technology offers another alternative to the design of compact integrated passive devices (IPDs) [26,27], and the RF MEMS devices are superior in aspects of tuning, switching, and integration with other

chips [28,29]. However, it is difficult for most of the above technologies to further shrink the footprints of filters to satisfy the increasing demands for the miniaturization of future electronic systems.

Three-dimensional (3D) integration and interposer technologies have emerged as effective solutions to the heterogeneous integration of multiple devices and chips [30–32]. As the core of 3D integration and interposer technologies, through-silicon-vias (TSVs) can vertically transmit electrical signals among different device layers, enabling high-performance systems within more compact areas [33–35]. Moreover, TSVs can also constitute several functional devices, such as capacitors [36] and inductors [37,38]. For RF applications, glass substrate is also used due to its high electrical resistivity and low electrical loss, where through-glass-vias (TGVs) are developed similar to TSVs [39,40]. Some of the reported literature has used TSV/TGV based capacitors together with inductors fabricated by traditional integrated circuit (IC) processes (or vice versa) to form BPF structures [41–44], showing great potential to improve the compactness of filters. To further simplify the device structure and reduce the process complexity, a compact, fully TGV-based BPF is proposed in [45]. Nevertheless, the manufacture of TGVs is not as mature as that of TSVs, which is more flexible and reliable in fabrication processes such as via etching and metalization. On the other hand, TSV technology has been widely studied and has achieved various progresses, for example, some low dielectric constant polymers are developed as substitutes for conventional SiO₂ liners, which feature low parasitic capacitance, good insulation quality, and low fabrication cost and complexity [46–48]. In this paper, novel and compact IPD structures including capacitor, inductor, and BPF are designed based on TSV technology. High resistivity silicon (HRS) with a resistivity of $1 \times 10^4 \Omega \cdot \text{cm}$ is used as the substrate has higher RF performance, as well as a better capability to be integrated with other Si based devices. Besides, polyimide (PI) is applied as the TSV liners, which can offer good electrical performance and be easily fabricated by a low-cost and simple technique named vacuum-assisted spin coating [49–51]. The electrical characteristics of the TSV based coaxial-like capacitors and solenoid inductors are discussed in detail. Notably, the utilized TSVs are identical and thus can be fabricated in a single batch. Employing the TSV based capacitor and inductor elements, a compact BPF structure is designed and evaluated, which possesses several attractive advantages, particularly with respect to a small footprint, simple structure, and low cost.

This paper is organized as follows: Sections 2 and 3 discuss the influences of design parameters on the performance of the TSV based coaxial-like capacitors and the TSV based solenoid inductors, respectively. Section 4 describes the modeling and characterization of the proposed BPF. Finally, the conclusions are summarized in Section 5.

2. TSV Based Coaxial-like Capacitor

Traditional on-chip capacitors are usually planar metal-insulator-metal (MIM) structures occupying large device areas. By sequentially depositing multiple layers via holes, 3D MIM capacitors named through-silicon-capacitors (TSCs) are fabricated [52–54]. Even though the TSCs have a smaller footprint than traditional planar capacitors, their fabrication processes are relatively complex. Actually, the TSV structure is a natural metal-insulator-semiconductor (MIS) capacitor, although the capacitance is always regarded as an unwanted parasitic parameter. Besides, if one TSV is placed at the center of several annularly arranged TSVs that are connected together, a coaxial-like capacitor structure can be formed, where the central conductor of the inner TSV and the central conductors of the surrounding TSVs act as the two terminals of the capacitor [55], respectively.

Based on the low-cost PI-TSV technology, a topological coaxial-like capacitor structure is firstly proposed, and the basic capacitor element comprised of five identical TSVs is shown in Figure 1. The HRS substrate is hidden for better observation. The TSVs have a diameter of 30 μm and a height of 300 μm , the thickness of PI liner is 0.5 μm , and the pitch between inner and outer TSVs is $25\sqrt{2}$ μm as the pitch between adjacent outer TSVs is set to be 50 μm . It can be seen that four surrounding TSVs are connected to a port by a backside

Cu redistribution layer (RDL), and the central TSV is linked to the other port by a frontside RDL. Actually, more surrounding TSVs contributes to increasing the capacitance of the coaxial-like capacitor [55], however, to build capacitors that have specific capacitances, the number of surrounding TSVs is set to be four, forming a square shape that can be easily duplicated.

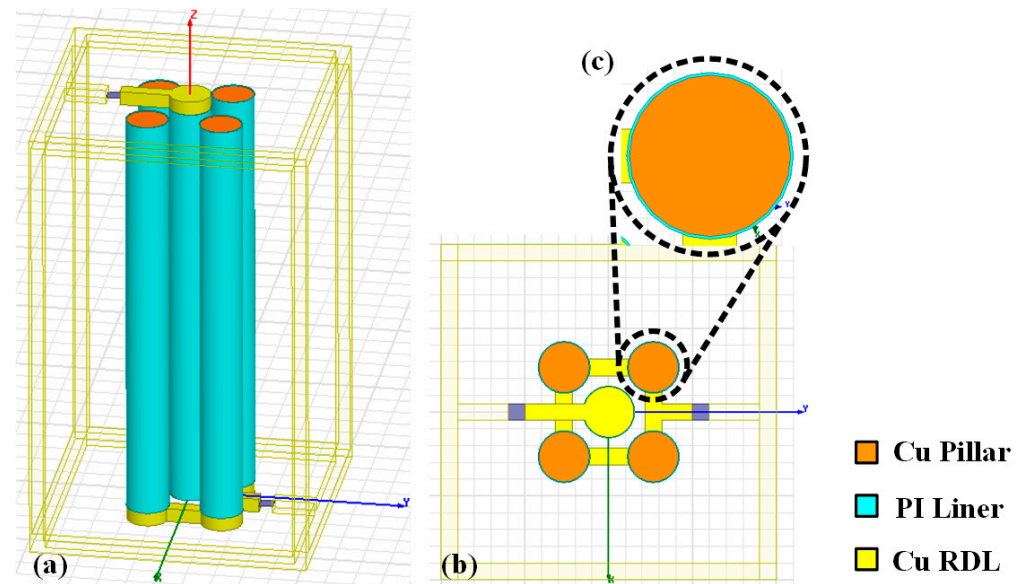


Figure 1. Basic capacitor element for the PI-TSV based coaxial-like capacitor structure: (a) side view, (b) top view, (c) is the enlarged image of a single TSV in (b).

Considering the sandwiched substrate between the inner and surrounding TSVs, the capacitance of such a coaxial-like capacitor is formed by the series connection of the parasitic capacitances of the inner TSV, the capacitance of the HRS substrate, and the parasitic capacitances of the surrounding TSVs. Therefore, the total capacitance of the capacitor element is influenced by the structural parameters of the TSVs and the pitch between central and outer TSVs.

Figure 2 plots the simulated capacitance–frequency characteristics of the capacitor element in Figure 1 under various design parameters, including TSV height, TSV diameter, thickness of PI liner, and pitch between inner and outer TSVs. As shown in Figure 2a,b, the increases in TSV height and diameter enlarge the capacitances over the simulated frequencies, due to the increased equivalent terminal areas in the capacitor. In addition, with the decreases in PI thickness and pitch between inner and outer TSVs, the parasitic capacitances of the PI-TSVs and the capacitance of the substrate are increased, respectively, leading to the increase in the total capacitance.

Moreover, arrays of coaxial-like capacitors with larger capacitances can be easily formed by the duplication and parallel connection of the basic square capacitor elements in both X- and Y-directions, which can be described as the matrix topology of coaxial-like capacitors.

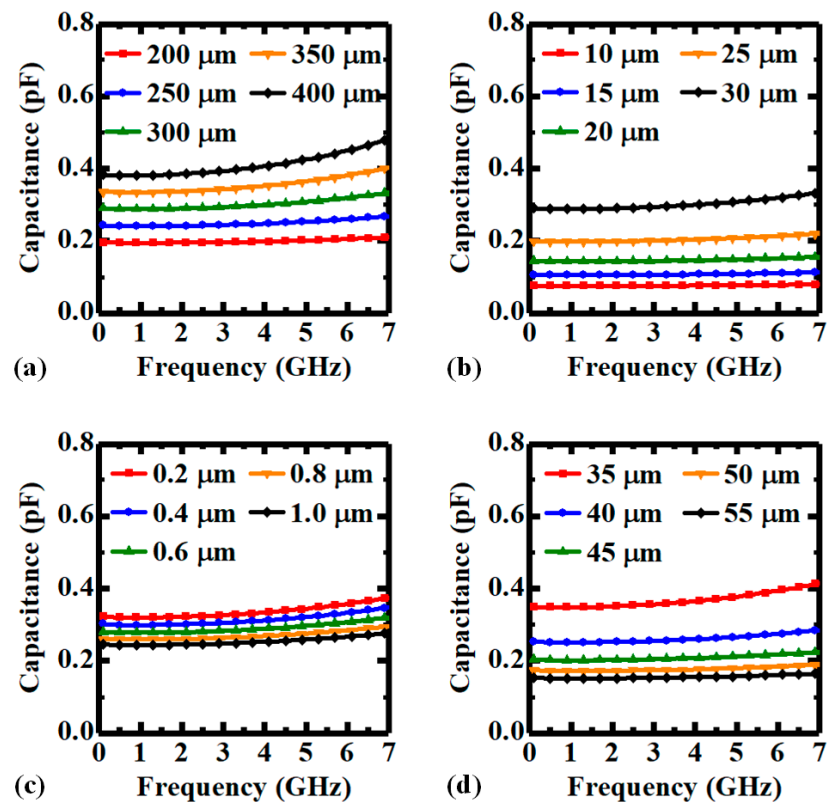


Figure 2. Capacitance–frequency characteristics of the PI-TSV based capacitor element with various (a) TSV heights, (b) TSV diameters, (c) thicknesses of PI liner, and (d) pitches between inner and outer TSVs.

3. TSV Based Solenoid Inductor

Three-dimensional (3D) solenoid inductors comprised of TSVs/TGVs and RDLs have been proposed for a smaller footprint and higher inductance density than traditional planar spiral structures [39,40]. To further reduce the manufacturing cost and complexity, a new 3D solenoid inductor structure based on low-cost PI-TSVs and corresponding RDLs is designed, and the basic inductor element with two turns is shown in Figure 3. The physical parameters of the PI-TSVs are the same as those of the coaxial-like capacitor in Section 2. It is shown that two X-directional adjacent TSVs and the RDLs form an equivalent coil, and the equivalent cross-sectional area of the inductor is decided by the pitch between the two TSVs and the TSV height. Actually, 3D solenoid inductors can store magnetic field energy more efficiently than planar structures, thus achieving larger quality factors within smaller footprints [39]. On the other hand, the pitch between two adjacent Y-directional TSVs acts as the loop pitch of the inductor, thus influencing the performance of the inductor together with the cross-sectional area and the number of turns. Therefore, the impact of various structural parameters including TSV height, TSV diameter, thickness of PI liner, and pitches between two adjacent TSVs in X- and Y-directions on the inductance and quality factor of the inductor element is analyzed, and the simulated results are shown in Figures 4 and 5.

Figure 4a shows that the inductance increases with TSV height as the cross-sectional area of the inductor increases. Besides, as the frequency-dependent alternating current (AC) resistance also increases with TSV height, the variation trend of the quality factor is determined by the weights of the increasing ratios of the reactance and the resistance at various frequencies. Therefore, the quality factor increases with TSV height at lower frequencies but decreases at higher frequencies, as shown in Figure 5a. As the increase in TSV diameter decreases the effective cross-sectional area, the inductance is declined accordingly, as shown in Figure 4b. However, as the resistance is decreased more significantly, the quality factor is increased instead, as shown in Figure 5b. Figures 4c and 5c

illustrate that the thickness of PI liner has little impact on the inductance and quality factor of the inductor element, which is because both the effective cross-sectional area and the resistance are almost unchanged, and the reduction in energy loss with thicker liner is not significant. As shown in Figure 4d, the influence of the pitch between two X-directional TSVs on the inductance is similar to that of the TSV height as both of them directly decide the effective cross-sectional area of the inductor. Notably, as the pitch between the two TSVs has less impact on the resistance of the coil compared to the TSV height, the quality factor is increased with the inductance, as shown in Figure 5d. Finally, the pitch between two Y-directional adjacent TSVs is actually influencing the equivalent length of the inductor, therefore, the inductance is slightly decreased with larger pitch, as shown in Figure 4e. On the other hand, as the inductive coupling is also decreased due to proximity effect, the quality factor is nearly the same, as shown in Figure 5e.

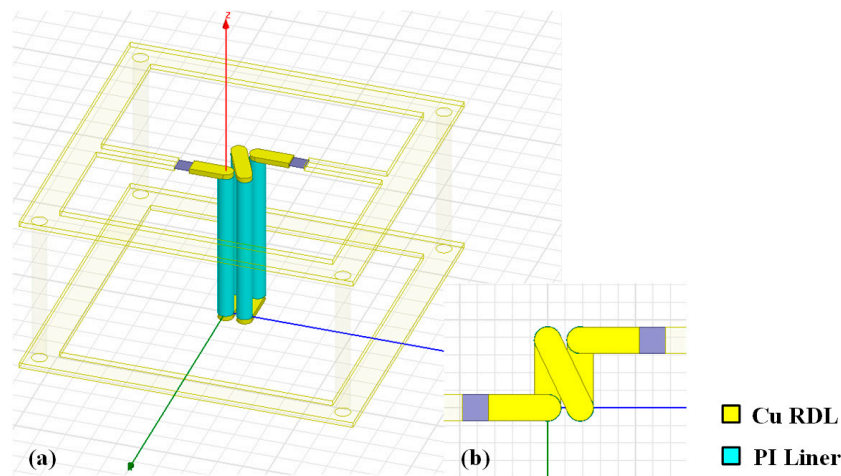


Figure 3. Basic inductor element for the PI-TSV based solenoid inductor structure: (a) side view, (b) top view.

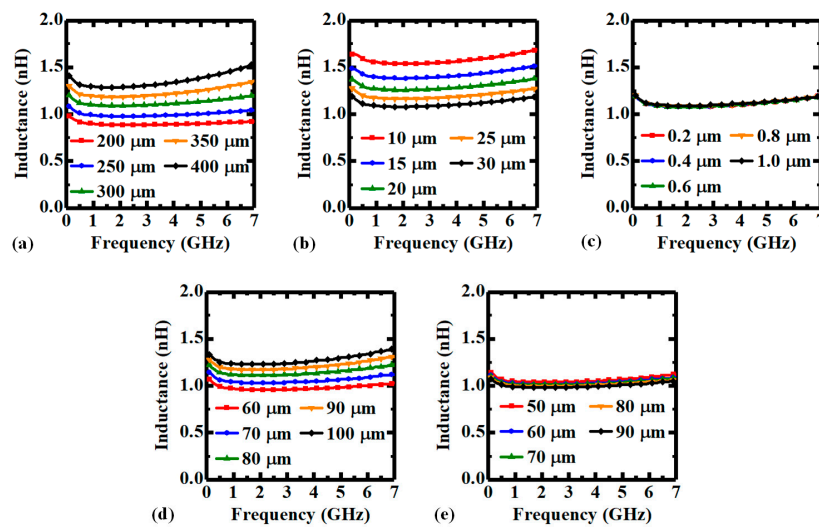


Figure 4. Inductance–frequency characteristics of the PI-TSV based inductor element with various (a) TSV heights, (b) TSV diameters, (c) thicknesses of PI liner, (d) pitch between two X-directional adjacent TSVs, and (e) pitch between two Y-directional adjacent TSVs.

Similar to the coaxial-like capacitor in Section 2, the basic solenoid inductor element can also constitute inductors with larger inductances in a simple topological method. As the proposed inductor element is composed of repeatable loops of identical TSVs and RDLs, an array of $2 \times N$ TSVs can easily be formed to multiply the inductance, where N refers to

the number of turns. Besides, the pitches between two adjacent TSVs in X- and Y-directions can also be adjusted to tune the inductance of the basic inductor element.

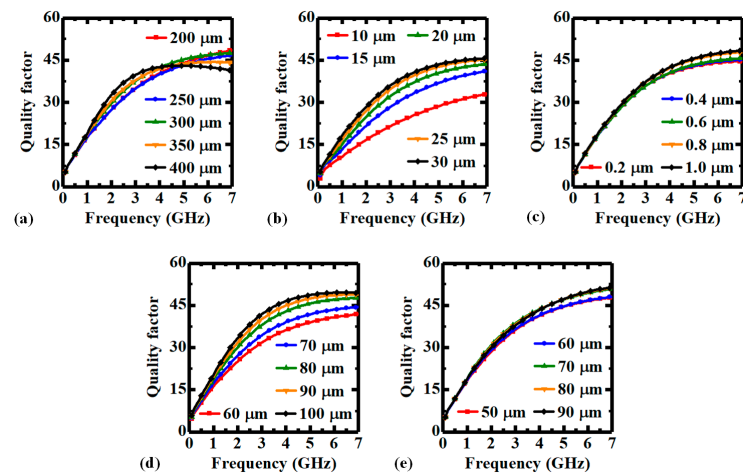


Figure 5. Quality factor-frequency characteristics of the PI-TSV based inductor element with various (a) TSV heights, (b) TSV diameters, (c) thicknesses of PI liner, (d) pitch between two X-directional adjacent TSVs, and (e) pitch between two Y-directional adjacent TSVs.

4. TSV Based Bandpass Filter

Based on the proposed coaxial-like capacitor and solenoid inductor structures, a novel BPF structure is designed, which is fully comprised of identical low-cost PI-TSVs. A typical prototype of third-order Butterworth BPF is adopted and the simplified circuit model of the designed filter with a central frequency (f_0) of 2.4 GHz is shown in Figure 6. Three capacitors and three inductors are used in the filter, and the parameter values of the components are derived and validated by the Keysight ADS circuit simulator. To obtain PI-TSV based capacitors and inductors of specific values, the coaxial-like capacitor element and the solenoid inductor element are topologically evolved.

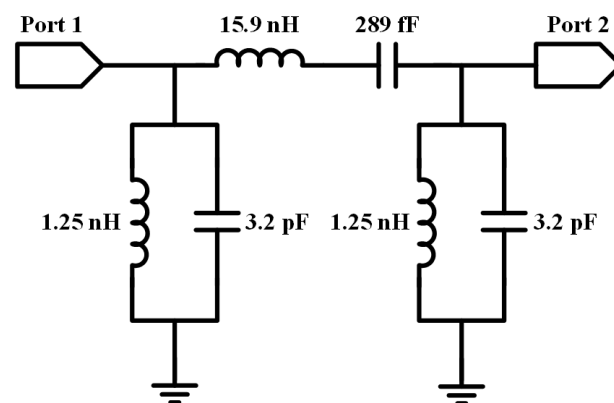


Figure 6. Circuit model of the proposed third-order Butterworth BPF.

Figure 7 shows the designed PI-TSV based BPF structure that is assembled by three arrays of coaxial-like capacitors and three 3D solenoid inductors with multi-turns. Notably, all TSVs in the filter are identical thus can be fabricated simultaneously, which greatly reduces the manufacturing cost and complexity. Moreover, as shown in Figure 7b, the footprint of the compact BPF is only 0.814 mm × 0.444 mm excluding the surrounding test framework, corresponding to an ultra-small electrical dimension of about 0.0065 λ_0 × 0.0035 λ_0 .

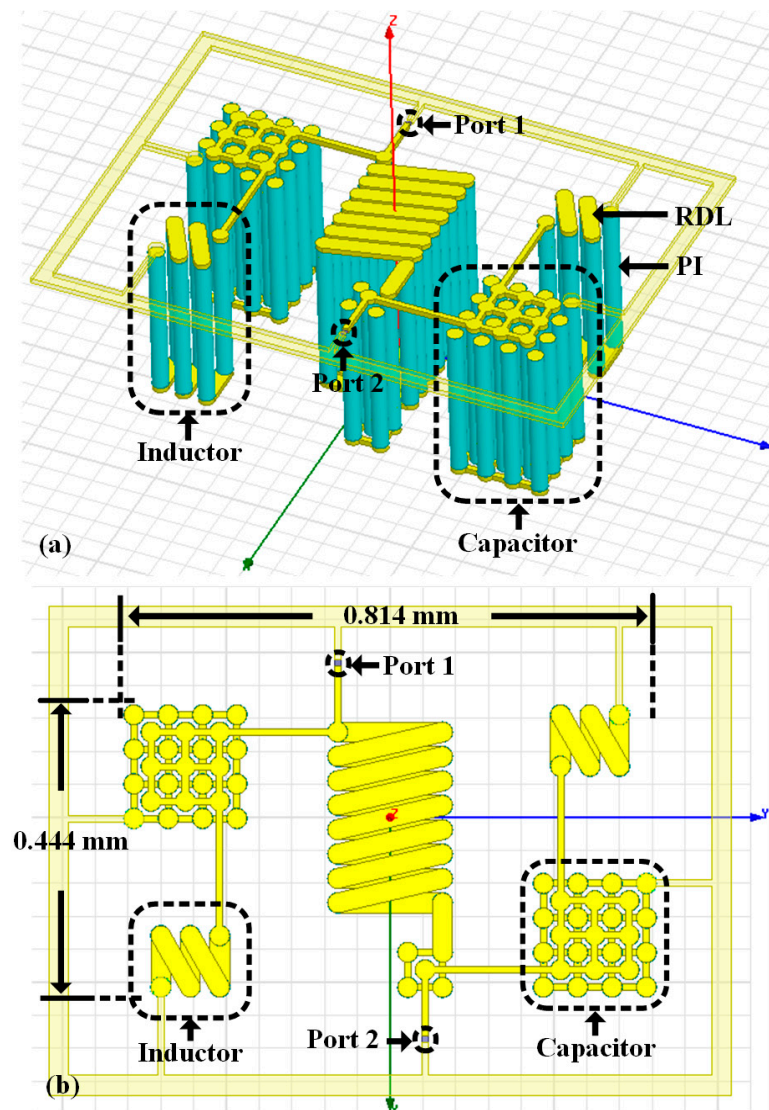


Figure 7. Structure of the proposed PI-TSV based BPF: (a) side view, (b) top view. A coaxial-like capacitor component and a solenoid inductor component are indicated. The device footprint is 0.814 mm \times 0.444 mm.

The transmission characteristics of the proposed BPF are analyzed using full-wave simulations in Ansys HFSS, and the return loss (S_{11}) and insertion loss (S_{21}) curves are plotted in Figure 8. Besides, the S_{11} and S_{21} curves obtained from the theoretical circuit model are also shown in Figure 8 for comparison. According to the simulated results, the f_0 of the BPF is 2.4 GHz, the 3-dB bandwidth is 410 MHz, and the fraction bandwidth (FBW) is 17%. In addition, the in-band insertion loss is less than 2.63 dB, and the return loss in the passband is better than 11.4 dB, showing good RF performance. Note that there are some deviations between the S-parameter curves of the circuit model and the physical model of the proposed PI-TSV based filter, which can be attributed to the parasitic parameters introduced by the TSV and RDL structures.

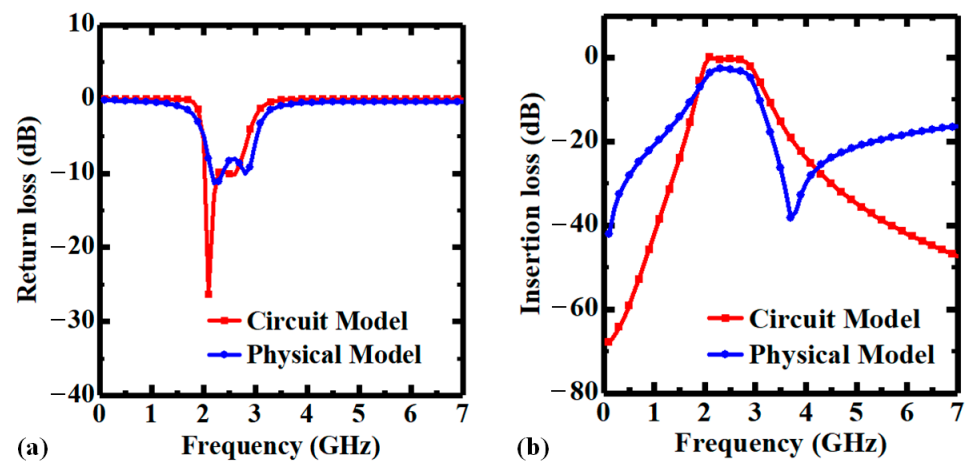


Figure 8. Transmission characteristics of the proposed PI-TSV based BPF: (a) return loss (S_{11}), (b) insertion loss (S_{21}). The red lines are obtained from the ideal circuit model, and the blue lines are simulated results of the physical model in HFSS.

Table 1 presents the comparisons of the designed PI-TSV based BPF with other published works in respect of RF characteristics, device sizes, technologies, and manufacturing costs and complexities. It is shown that the proposed compact PI-TSV based BPF has comparable RF performance with the state-of-the-art designs, while it occupies a smaller footprint than most of the reported ones. Even though that the filter in [44] has an even smaller size, its fabrication flow is relatively complex as it stacks several parallel plate capacitors on the TGV based inductors. Moreover, as the proposed filter in this work is developed based on a single Si interposer with a thickness of 300 μm and is fully formed by low-cost PI-TSV structures and corresponding RDLs, it is able to be fabricated by the relatively mature TSV technology without the need to introduce extra bonding steps or IC processes. Meanwhile, all TSVs can be synchronously fabricated within one process round, which further reduces the manufacture cost and complexity. Besides, the PI-TSV based BPF is also attractive in the modern RF/electronic micro-systems as it is compatible with 3D integration technology and can be easily integrated with other chips and modules.

Table 1. Comparisons of the proposed BPF with other published designs.

References	f_0 (GHz)	FBW (%)	Insertion Loss (dB)	Return Loss (dB)	Size (mm \times mm)	Technology
[17]	2.4	12.5	2.4	15	2.63×2.61	LTCC
[18]	2.6	10.2	2.47	20	2×1.7	LTCC
[23]	2.4	174	1.1	11	87.5×12.8	SSPP
[43]	2.65	62.9	0.6	30	1×0.5	TGV and IC
[44]	2.45	31.5	2.4	15	0.44×0.33	TGV and IC
[56]	2.7	2	3.8	14	44.8×16	DPAM *
[57]	2.33	39.8	0.65	15	18.5×18.5	Micro-strip
[58]	2.4	10.4	0.87	15	9.4×23.1	Micro-strip
[59]	2.4	12.1	1.2	15	19.1×11.2	Micro-strip
This work	2.4	17	2.63	11.4	0.81×0.44	PI-TSV

* DPAM: Direct print additive manufacturing.

5. Conclusions

In this work, fully PI-TSV based IPDs including capacitor, inductor, and BPF are designed and evaluated. The impacts of various design parameters on the performance of the TSV based coaxial-like capacitor and the TSV based solenoid inductor are analyzed, providing a guidance to the development of such components. Capacitors and inductors with specific values of capacitances and inductances can be easily achieved by the topologies of the basic coaxial-like capacitor element and solenoid inductor element. Based on this

topological method, a novel compact BPF structure is proposed, which is composed of several arrays of coaxial-like capacitors and multi-turns solenoid inductors. The 3-dB bandwidth and the fraction bandwidth (FBW) of the filter is 410 MHz and 17%, respectively. Besides, the in-band insertion loss is less than 2.63 dB, and the return loss in the passband is better than 11.4 dB, showing good RF performance. Notably, the device size of the BPF is only $0.814 \text{ mm} \times 0.444 \text{ mm}$ ($0.0065 \lambda_0 \times 0.0035 \lambda_0$). Moreover, as the proposed BPF is fully formed by low-cost PI-TSVs with the same structural parameters and corresponding RDLs, it features lower manufacturing cost and complexity compared to other reported designs. Furthermore, the BPF is convenient to be integrated with other devices as it is built in a natural Si interposer structure. As a conclusion, the proposed design of compact BPF is promising for the miniaturization and integration of modern RF applications.

Author Contributions: Conceptualization, Y.D. and Z.Z.; methodology, M.Z. and Z.Z.; software, H.D., H.W., X.P. and M.Z.; validation, M.Z. and Z.Z.; formal analysis, H.D., Y.D., M.Z. and Z.Z.; investigation, H.D., H.W. and X.P.; resources, H.D., Y.D. and Z.Z.; data curation, H.W., X.P., M.Z. and Z.Z.; writing—original draft preparation, Z.Z.; writing—review and editing, H.D., Y.D. and Z.Z.; visualization, M.Z. and Z.Z.; supervision, Y.D. and Z.Z.; project administration, Y.D.; funding acquisition, Y.D. All authors have read and agreed to the published version of the manuscript.

Funding: This research was funded in part by the National Natural Science Foundation of China under Grants 62074015 and 61774015, and in part by the Beijing Nova Program of Science and Technology under Grant Z191100001119078.

Data Availability Statement: Not applicable.

Conflicts of Interest: The authors declare no conflict of interest.

References

1. Pourzadi, A.; Isapour, A.; Kouki, A. Design of Compact Dual-Band LTCC Second-Order Chebyshev Bandpass Filters Using a Direct Synthesis Approach. *IEEE Trans. Microw. Theory Techn.* **2019**, *67*, 1441–1451. [\[CrossRef\]](#)
2. Feng, W.; Gao, X.; Che, W.; Yang, W.; Xue, Q. LTCC Wideband Bandpass Filters with High Performance Using Coupled Lines with Open/Shorted Stubs. *IEEE Trans. Compon. Packag. Manuf. Technol.* **2017**, *7*, 602–609. [\[CrossRef\]](#)
3. Xiao, J.-K.; Zhu, M.; Li, Y.; Tian, L.; Ma, J.-G. High Selective Microstrip Bandpass Filter and Diplexer with Mixed Electromagnetic Coupling. *IEEE Microw. Wireless Compon. Lett.* **2015**, *25*, 781–783. [\[CrossRef\]](#)
4. Zhu, L.; Bu, H.; Wu, K. Aperture Compensation Technique for Innovative Design of Ultra-Broadband Microstrip Bandpass Filter. In Proceedings of the IEEE MTT-S International Microwave Symposium (IMS2000), Boston, MA, USA, 11–16 June 2000; pp. 315–318.
5. Mul, M.; Jasinski, M.; Lamecki, A.; Gómez-García, R.; Mrozowski, M. Inline Microwave Filters with N+1 Transmission Zeros Generated by Frequency-Variant Couplings: Coupling-Matrix-Based Synthesis and Design. *IEEE Trans. Circuits Syst. II Exp. Briefs* **2022**, *69*, 824–828. [\[CrossRef\]](#)
6. Zhang, W.; Gu, J.; Xu, G.; Luo, L.; Li, X. Copper/Benzocyclopentene Thin Film Technique Based Microstrip Bandpass Filter Featured by Thick Dielectric Layer for Low Insertion Loss. *Microw. Opt. Technol. Lett.* **2020**, *62*, 3695–3701. [\[CrossRef\]](#)
7. Huang, Y.; Shao, Z.; Liu, L. A Substrate Integrated Waveguide Bandpass Filter Using Novel Defected Ground Structure Shape. *Progr. Electromagn. Res.* **2013**, *135*, 201–213. [\[CrossRef\]](#)
8. Sánchez, J.R.; Bachiller, C.; Nova, V.; Boria, V.E. Controlled Out-of-Band Rejection of Filters based on SIW with Alternating Dielectric Line Sections. *IEEE Microw. Wireless Compon. Lett.* **2015**, *29*, 258–260. [\[CrossRef\]](#)
9. Shen, W.; Yin, W.-Y.; Sun, X.-W.; Wu, L.-S. Substrate-Integrated Waveguide Bandpass Filters with Planar Resonators for System-on-Package. *IEEE Trans. Compon. Packag. Manuf. Technol.* **2013**, *3*, 253–261. [\[CrossRef\]](#)
10. Dey, S.; Koul, S.K. Reliable, Compact, and Tunable MEMS Bandpass Filter Using Arrays of Series and Shunt Bridges for 28-GHz 5G Applications. *IEEE Trans. Microw. Theory Techn.* **2021**, *69*, 75–88. [\[CrossRef\]](#)
11. Shim, Y.; Wu, Z.; Rais-Zadeh, M. A High-Performance Continuously Tunable MEMS Bandpass Filter at 1 GHz. *IEEE Trans. Microw. Theory Techn.* **2012**, *60*, 2439–2447. [\[CrossRef\]](#)
12. Mahon, S. The 5G Effect on RF Filter Technologies. *IEEE Trans. Semicond. Manuf.* **2017**, *30*, 494–499. [\[CrossRef\]](#)
13. Lin, W.; Ziolkowski, R.W.; Huang, J. Electrically Small, Low-Profile, Highly Efficient, Huygens Dipole Rectennas for Wirelessly Powering Internet-of-Things Devices. *IEEE Trans. Antennas Propag.* **2019**, *67*, 3670–3679. [\[CrossRef\]](#)
14. Hunter, C.; Billonnet, L.; Jarry, B.; Guillon, P. Microwave Filters—Applications and Technology. *IEEE Trans. Microw. Theory Techn.* **2002**, *50*, 794–805. [\[CrossRef\]](#)
15. Liu, L.; Bai, T.-L.; Deng, J.-Y.; Sun, D.; Zhang, Y.; Yong, T.; Zhou, S.-G.; Guo, L.-Z. Substrate Integrated Waveguide Filtering Horn Antenna Facilitated by Embedded Via-Hole Arrays. *IEEE Antennas Wirel. Propag. Lett.* **2020**, *19*, 1187–1191. [\[CrossRef\]](#)

16. Zheng, Y.; Sheng, W. Compact Lumped-Element LTCC Bandpass Filter for Low-Loss VHF-Band Applications. *IEEE Microw. Wirless Compon. Lett.* **2017**, *27*, 1074–1076. [[CrossRef](#)]
17. Zhang, X.Y.; Dai, X.; Kao, H.-L.; Wei, B.-H.; Cai, Z.Y.; Xue, Q. Compact LTCC Bandpass Filter with Wide Stopband Using Discriminating Coupling. *IEEE Trans. Compon. Packag. Manuf. Technol.* **2014**, *4*, 656–663. [[CrossRef](#)]
18. Xu, J.-X.; Zhang, X.Y.; Zhao, X.-L.; Xue, Q. Synthesis and Implementation of LTCC Bandpass Filter with Harmonic Suppression. *IEEE Trans. Compon. Packag. Manuf. Technol.* **2016**, *6*, 596–604. [[CrossRef](#)]
19. Lai, Q.; Fumeaux, C.; Hong, W.; Vahldieck, R. Characterization of the Propagation Properties of the Half-Mode Substrate Integrated Waveguide. *IEEE Trans. Microw. Theory Techn.* **2009**, *57*, 1996–2004.
20. Huang, L.; Cha, H. Compact ridged half-mode substrate integrated waveguide bandpass filter. *IEEE Microw. Wirel. Compon. Lett.* **2015**, *25*, 223–225. [[CrossRef](#)]
21. Huang, L.; Cha, H.; Li, Y. Compact Wideband Ridge Half-Mode Substrate Integrated Waveguide Filters. *IEEE Trans. Microw. Theory Techn.* **2016**, *64*, 3568–3579. [[CrossRef](#)]
22. Zhao, L.; Zhang, X.; Wang, J.; Yu, W.; Li, J.; Su, H.; Shen, X. A Novel Broadband Band-pass Filter Based on Spoof Surface Plasmon Polaritons. *Sci. Rep.* **2016**, *6*, 36069. [[CrossRef](#)]
23. Wang, M.; Sun, S.; Ma, H.F.; Cui, T.J. Supercompact and Ultrawideband Surface Plasmonic Bandpass Filter. *IEEE Trans. Microw. Theory Techn.* **2020**, *68*, 732–740. [[CrossRef](#)]
24. Guan, D.-F.; You, P.; Zhang, Q.; Yang, Z.-B.; Liu, H.; Yong, S.-W. Slow-Wave Half-Mode Substrate Integrated Waveguide Using Spoof Surface Plasmon Polariton Structure. *IEEE Trans. Microw. Theory Techn.* **2018**, *66*, 2946–2952. [[CrossRef](#)]
25. Guan, D.-F.; You, P.; Zhang, Q.; Xiao, K.; Yong, S.-W. Hybrid Spoof Surface Plasmon Polariton and Substrate Integrated Waveguide Transmission Line and Its Application in Filter. *IEEE Trans. Microw. Theory Techn.* **2017**, *65*, 4925–4932. [[CrossRef](#)]
26. Lin, T.-W.; Low, K.K.W.; Gaddi, R.; Rebeiz, G.M. High-Linearity 5.3–7.0 GHz 3-Pole Tunable Bandpass Filter Using Commercial RF MEMS Capacitors. In Proceedings of the 2018 48th European Microwave Conference (EuMC), Madrid, Spain, 25–27 September 2018; pp. 555–558.
27. Hikmat, F.; Ali, M.S.M. RF MEMS Inductors and Their Applications—A Review. *J. Microelectromech. Syst.* **2017**, *26*, 17–44. [[CrossRef](#)]
28. Liu, X.; Katehi, L.P.B.; Chappell, W.J.; Peroulis, D. A 3.4–6.2 GHz Continuously Tunable Electrostatic MEMS Resonator with Quality Factor of 460–530. In Proceedings of the 2009 IEEE MTT-S International Microwave Symposium Digest, Boston, MA, USA, 7–12 June 2009; pp. 1149–1152.
29. Hafiz, M.A.A.; Kosuru, L.; Hajjaj, A.Z.; Younis, M.I. Highly Tunable Narrow Bandpass MEMS Filter. *IEEE Trans. Electron. Devices.* **2017**, *64*, 3392–3398. [[CrossRef](#)]
30. Koyanagi, M. Heterogeneous 3D Integration—Technology Enabler Toward Future Super-Chip. In Proceedings of the 2013 IEEE International Electron Devices Meeting, Washington, DC, USA, 9–11 December 2013; pp. 1.2.1–1.2.8.
31. Beica, R. 3D Integration: Applications and Market Trends. In Proceedings of the 2015 International 3D Systems Integration Conference (3DIC), Sendai, Japan, 31 August–2 September 2015; pp. TS5.1.1–TS5.1.7.
32. Beyne, E. The Rise of the 3rd Dimension for System Integration. In Proceedings of the 2006 International Interconnect Technology Conference, Burlingame, CA, USA, 5–7 June 2006; pp. 1–5.
33. Wang, Z. 3-D integration and through-silicon vias in MEMS and microsensors. *J. Microelectromech. Syst.* **2015**, *24*, 1211–1244. [[CrossRef](#)]
34. Lau, J.H. *Through-Silicon Vias for 3D Integration*; McGraw-Hill: New York, NY, USA, 2012.
35. Motoyoshi, M. Through-Silicon Via (TSV). *Proc. IEEE* **2009**, *97*, 43–48. [[CrossRef](#)]
36. Chang, Y.-Y.; Ko, C.-T.; Yu, T.-H.; Hsieh, Y.-S.; Chen, K.-N. Modeling and Characterization of TSV Capacitor and Stable Low-Capacitance Implementation for Wide-I/O Application. *IEEE Trans. Device Mater. Rel.* **2015**, *15*, 129–135. [[CrossRef](#)]
37. Tian, U.R.; Yang, R.; Zhuo, C.; Shi, Y. On the Efficacy of Through-Silicon-via Inductors. *IEEE Trans. Very Large Scale Integr. (VLSI) Syst.* **2015**, *23*, 1322–1334.
38. Li, H.; Liu, J.; Xu, T.; Xia, J.; Tan, X.; Tao, Z. Fabrication and Optimization of High Aspect Ratio Through-Silicon-Vias Electroplating for 3D Inductor. *Micromachines* **2018**, *9*, 528. [[CrossRef](#)] [[PubMed](#)]
39. Kim, J.; Shenoy, R.; Lai, K.-Y.; Kim, J. High-Q 3D RF Solenoid Inductors in Glass. In Proceedings of the 2014 IEEE Radio Frequency Integrated Circuits Symposium, Tampa, FL, USA, 1–3 June 2014; pp. 199–200.
40. Kim, M.S.; Pulugurtha, M.R.; Sundaram, V.; Tummala, R.R.; Yun, H. Ultrathin High-Q 2-D and 3-D RF Inductors in Glass Packages. *IEEE Trans. Compon. Packag. Manuf. Technol.* **2018**, *8*, 643–652. [[CrossRef](#)]
41. Yook, J.-M.; Kim, D.; Kim, J.C. High-Q Trenched Spiral Inductors and Low-loss Low Pass Filters Using through Silicon via Processes. *Jpn. J. Appl. Phys.* **2014**, *53*, 04EE11. [[CrossRef](#)]
42. Wang, F.; Yu, N. An Ultracompact Butterworth Low-Pass Filter Based on Coaxial Through-Silicon Vias. *IEEE Trans. Very Large Scale Integr. (VLSI) Syst.* **2017**, *25*, 1164–1167. [[CrossRef](#)]
43. Sitaraman, S.; Sukumaran, V.; Pulugurtha, M.R.; Wu, Z.; Suzuki, Y.; Kim, Y.; Sundaram, V.; Kim, J.; Tummala, R.R. Miniaturized Bandpass Filters as Ultrathin 3-D IPDs and Embedded Thinfilms in 3-D Glass Modules. *IEEE Trans. Compon. Packag. Manuf. Technol.* **2017**, *7*, 1410–1418. [[CrossRef](#)]
44. Qian, L.; Sang, J.; Xia, Y.; Wang, J.; Zhao, P. Investigating on Through Glass via Based RF Passives for 3-D Integration. *IEEE J. Electron. Devices Soc.* **2018**, *6*, 755–759. [[CrossRef](#)]

45. Zhang, Z.; Ding, Y.; Chen, Z.; Zhou, M.; Xiao, L.; Cai, Z.; Xiong, M.; Gong, X. Design and Evaluation of a Novel and Ultra-Compact Fully-TGV-Based Self-Shielding Bandpass Filter for 5G Applications. In Proceedings of the 2019 International 3D Systems Integration Conference (3DIC), Sendai, Japan, 8–10 October 2019; pp. 1–4.
46. Mariappan, M.; Fukushima, T.; Beatrix, J.; Hashimoto, H.; Sato, Y.; Lee, K.; Tanaka, T.; Koyanagi, M. Replacing the PECVD-SiO₂ in the Through-Silicon Via of High-Density 3D LSIs with Highly Scalable Low Cost Organic Liner: Merits and Demerits. In Proceedings of the 2014 IEEE 64th Electronic Components and Technology Conference (ECTC), Orlando, FL, USA, 27–30 May 2014; pp. 636–640.
47. Chen, Q.; Cui, H.; Tan, Z.; Wang, Z. Low Capacitance Through-Silicon-Vias with Uniform Benzocyclobutene Insulation Layers. *IEEE Trans. Compon. Packag. Manuf. Technol.* **2013**, *3*, 724–731. [[CrossRef](#)]
48. Liu, B.; Yan, Y.; Zhang, Z.; Chen, Z.; Ding, Y. Electrical Characteristics and Thermal Reliability of Blind Through-Silicon-Vias with Polyimide Liners. In Proceedings of the 2016 17th International Conference on Electronic Packaging Technology (ICEPT), Wuhan, China, 16–19 August 2016; pp. 1360–1364.
49. Yan, Y.; Ding, Y.; Chen, Q.; Lee, K.; Fukushima, T.; Koyanagi, M. Vacuum-Assisted-Spin-Coating of Polyimide Liner for High-Aspect-Ratio TSVs Applications. In Proceedings of the 2015 International 3D Systems Integration Conference (3DIC), Sendai, Japan, 31 August–2 September 2015; pp. TS5.2.1–TS5.2.5.
50. Yan, Y.; Zhang, Z.; Cheng, Z.; Zhou, L.; Chen, Z.; Ding, Y. Low Cost Polyimide Liner Formation with Vacuum-Assisted Spin Coating for Through-Silicon-Vias. In Proceedings of the 2016 IEEE International 3D Systems Integration Conference (3DIC), San Francisco, CA, USA, 8–11 November 2016; pp. 1–5.
51. Xiong, M.; Chen, Z.; Ding, Y.; Kino, H.; Fukushima, T.; Tanaka, T. Development of Eccentric Spin Coating of Polymer Liner for Low-Temperature TSV Technology with Ultra-Fine Diameter. *IEEE Electron. Device Lett.* **2019**, *40*, 95–98. [[CrossRef](#)]
52. Guiller, O.; Joblot, S.; Lamy, Y.; Farcy, A.; Carpentier, J.F.; Defay, E. Through Silicon Capacitor Co-Integrated with TSVs on Silicon Interposer. *Microelectron. Eng.* **2014**, *20*, 121–126. [[CrossRef](#)]
53. Li, J.; Ma, S.; Liu, H.; Guan, Y.; Chen, J.; Jin, Y.; Wang, W.; Hu, L.; He, S. Design, Fabrication and Characterization of TSV Interposer Integrated 3D Capacitor for SIP Applications. In Proceedings of the 2018 IEEE 68th Electronic Components and Technology Conference (ECTC), San Diego, CA, USA, 29 May–1 June 2018; pp. 1974–1980.
54. Lin, Y.; Li, H.Y.; Tan, C.S. Structural Integrity of 3-D Metal-Insulator-Metal Capacitor Embedded in Fully Filled Cu Through-Silicon Via. *IEEE Trans. Compon. Packag. Manuf. Technol.* **2021**, *11*, 918–921. [[CrossRef](#)]
55. Lu, K.-C.; Horng, T.-S.; Li, H.-H.; Fan, K.C.; Huang, T.-Y.; Lin, C.-H. Scalable Modeling and Wideband Measurement Techniques for a Signal TSV Surrounded by Multiple Ground TSVs for RF/High-Speed Applications. In Proceedings of the 2012 IEEE 62nd Electronic Components and Technology Conference, San Diego, CA, USA, 29 May–1 June 2012; pp. 1023–1026.
56. Hawatmeh, D.; Weller, T. 2.4 GHz Band Pass Filter Architecture for Direct Print Additive Manufacturing. In Proceedings of the 2018 IEEE/MTT-S International Microwave Symposium—IMS, Philadelphia, PA, USA, 10–15 June 2018; pp. 67–70.
57. Xu, J. Compact Quasi-Elliptic Response Wideband Bandpass Filter with Four Transmission Zeros. *IEEE Microw. Wireless Compon. Lett.* **2015**, *25*, 169–171. [[CrossRef](#)]
58. Belmajdoub, A.; El Alami, A.; Das, S.; Madhav, B.T.P.; Bennani, S.D.; Jorio, M. Design, Optimization and Realization of Compact Bandpass Filter Using Two Identical Square Open-Loop Resonators for Wireless Communications Systems. *Int. J. Instrum. (IJINST)* **2019**, *14*, 09012. [[CrossRef](#)]
59. Afzali, B.; Abbasi, H.; Shama, F.; Dehdasht-Heydari, R. A Microstrip Bandpass Filter with Deep Rejection and Low Insertion Loss for Application at 2.4 GHz Useful Wireless Frequency. *Int. J. Electron. Commun.* **2021**, *138*, 153811. [[CrossRef](#)]

Disclaimer/Publisher’s Note: The statements, opinions and data contained in all publications are solely those of the individual author(s) and contributor(s) and not of MDPI and/or the editor(s). MDPI and/or the editor(s) disclaim responsibility for any injury to people or property resulting from any ideas, methods, instructions or products referred to in the content.